ACH – MODELS IN CHEMISTRY 134 (5), 573–594 (1997)

Fourier transform of molecular spectra versus classical periodic orbits. The example of CO_2

MARC JOYEUX and LAURENT MICHAILLE

Laboratoire de Spectrométrie Physique (CNRS UMR 5588), Université Joseph Fourier - Grenoble I, BP 87, 38402 St Martin d'Hères Cedex, France

Received June 5, 1996

Periodic orbits are those classical trajectories, which exactly loop after a finite time called precisely the period of the periodic orbit. Semiclassical trace formulae connect classical dynamics to quantum spectra, by showing that the peaks, which appear in the Fourier transform of a spectrum, correspond to the periods of the periodic orbits of the underlying classical system. At short times, where peaks are still well separated in the Fourier transform of the spectrum, one is then able, at least theoretically, to assign a classical periodic orbit to each peak. This article deals with the assignment of the Fourier transform of the vibrational spectrum of CO_2 up to 300 femtoseconds, using Berry and Tabor's trace formula for integrable (non chaotic) systems. Since analytical expressions are known for the action integrals and classical frequencies of two vibrational modes in Fermi interaction, one gets a clear picture of what happens. In particular, the similarities and the differences, which are observed between the Fourier transforms of the 2D and 3D spectra of CO_2, the former one being obtained by freezing the antisymmetric stretching degree of freedom, can be analysed in some detail.

Introduction

The Fourier transform (FT) of a quantum spectrum may reveal the chaotic behaviour of the underlying classical system through the appearance of the so-called correlation hole [1–2]. Since the correlation hole fills up at a time corresponding to the average density of states, this information must generally be sought for at rather large time values for the vibrations of a triatomic molecule (an average density of states of 0.1 level/cm^{-1} is associated with a time of 3 ps).

Nonetheless, some information concerning the dynamics of the underlying classical system is also contained in the FT of the spectrum at time scales much shorter than the average density of states. The key result is that peaks appear in the FT at those values of time, which correspond to the periods of the classical periodic orbits (POs). At short times, peaks are well separated in the FT, and one is *a priori*

1217-8969/97/ $ 5.00

able to assign a classical PO to each peak. In this paper, we propose to assign the FT of the vibrational spectrum of CO_2 for times up to about 300 femtoseconds.

The connection between quantum and classical mechanics consists of the so-called trace formulae, which express the semiclassical density of states (that is, the spectrum with peak intensity normalised to 1), as a function of the properties of the classical POs. There exist at least three trace formulae, each one applying to a particular type of system. Berry and Tabor's trace formula [3], applies to regular (non chaotic) systems [3, 4]. At the opposite, Gutzwiller's trace formula [5–7] is valid for completely chaotic systems [8–14]. The gap between these two formulae is in part filled by the trace formula for mixed systems, which has been worked out by Ozorio de Almeida [15] and Tomsovic, Grinberg and Ullmo [16].

The limiting step when looking forward to apply a trace formula consists precisely in finding the classical POs. This usually requires a large amount of numerical calculations. An exception occurs for integrable systems, that is for Berry and Tabor's trace formula, whenever one is able to calculate analytically the classical frequencies of the system. Unfortunately, Berry and Tabor's trace formula only marginally applies to the most widely used, regular and analytically soluble molecular Hamiltonian, that is the polynomial Dunham expansion, because of the almost complete lack of curvature of the energy surface [3]. In contrast, it correctly applies to the Hamiltonian, which describes two vibrational modes in Fermi resonance, like the bending and symmetric stretching modes of CO_2, because of the strong curvature of the energy surface which is induced by the separatrix [17]. In addition, analytical expressions have recently been given for the classical frequencies and action integrals of this Hamiltonian [18, 19], so that all the tools, which are needed to connect the classical POs of CO_2 to the FT of its vibrational spectrum and to have a clear understanding of what happens are at one's disposal.

Other recent articles dealing with the connection between classical POs and molecular spectra include the very complete review article of Gaspard et al., entitled *New ways of understanding semiclassical quantization* [20], two papers of Ezra [21] and Rouben and Ezra [22], who study the same type of resonance Hamiltonian as we do, an article of Hirai et al. [23], who discuss several examples available from experimental spectra, and a more theoretical article of Baranger et al. [24], where the results obtained for further model Hamiltonians are presented.

Action integrals, classical frequencies and POs

The classical Hamiltonian H describing a system with N degrees of freedom is expressed as a function of N generalised coordinates q_i and their N conjugate momenta p_i. If the system is regular (non chaotic), then each trajectory is characterised by N constants of the motion $\mathcal{I}_i$, which are called action integrals and are calculated according to [25]:

$$\mathcal{I}_i = \frac{1}{2\pi} \oint_{C_i} \sum_{k=1}^{N} p_k \, \mathrm{d}q_k \, . \tag{1}$$

The paths C_i in Eq. (1) are N closed loops, which are topologically equivalent to the N principal circles of the torus supporting the trajectory. The energy of the system can be rewritten as a function of the N action integrals:

$$E \equiv H(p_1,q_1,\ldots,p_N,q_N) \equiv H(\mathcal{I}_1,\ldots,\mathcal{I}_N) \, . \tag{2}$$

Associated with each action integral is a classical frequency W_i, defined according to:

$$W_i = \frac{\partial H(\mathcal{I}_1,\ldots,\mathcal{I}_N)}{\partial \mathcal{I}_i} \, . \tag{3}$$

Each classical observable defined on the trajectory, like for instance individual coordinates q_i or p_i, can then be Fourier expanded in terms of the sole combinations and overtones of the N classical frequencies W_i. On the other hand, periodic orbits (POs) are those trajectories that exactly loop after a finite time T, called the period of the PO. A trajectory, such that the N classical frequencies are rationally related, i.e., such that:

$$\exists (\mu_1, \ldots, \mu_N) \in N^N, \qquad \frac{\mu_1}{W_1} = \ldots = \frac{\mu_N}{W_N} = \frac{T_\mu}{2\pi} \tag{4}$$

is associated with a so-called rational torus and is obviously a PO with period T_μ. Hereafter, these POs will also be called N-dimensional POs (or ND POs), because particles actually experience motion along the N angles of the rational torus. In contrast, there exist other POs, which will be described as $(N-n)$-dimensional POs (or $(N-n)$D POs) and are characterised by n vanishing amplitudes of motion along the frequencies $W_1,\ldots,W_n$ and $N-n-1$ proportionality relations similar to Eq. (4) along the frequencies $W_{n+1},\ldots,W_N$.

Berry and Tabor's trace formula

For integrable systems, Berry and Tabor's trace formula [3] connects the density of states, that is the spectrum with peaks normalised to 1, to a sum involving the rational tori of the classical system. To be exact, the density of states $n(E)$, which appears in the trace formula is the semiclassical density of states resulting from Einstein–Brillouin–Keller (EBK) quantization. However, for the Hamiltonian, which describes vibrational modes in near $1:n$ resonance (see Eqs (16) and (28)), the quantum and semiclassical energy levels are very close together even for low-lying levels [17–19, 26, 27]. This is the reason, why the trace formula can be viewed as the connection between the quantum spectrum and the dynamics of the underlying classical Hamiltonian.

In the case of an Hamiltonian with N degrees of freedom, the simplest trace formula given in Eq. (21) of [3] is:

$$n(E) \approx \sum_{\substack{\text{rational} \\ \text{tori}(\mu)\text{at}E}} A_\mu \cos(2\pi\mu\mathfrak{I}_\mu - \frac{\pi}{2}\mu\alpha + \frac{\pi}{4}\beta_\mu) , \tag{5}$$

where $\mu = (\mu_1, \ldots, \mu_N)$, $\mathfrak{I}_\mu = (\mathfrak{I}_1, \ldots, \mathfrak{I}_N)$ computed at the rational tori, $\alpha = (\alpha_1, \ldots, \alpha_N)$ is the vector of the Maslov indexes and β_μ is the signature computed at the rational tori of a matrix resulting from the stationary phase approximation. In the present work, α and β_μ will remain largely irrelevant. The amplitude term A_μ depends only on the classical properties (action integrals, classical frequencies, and derivatives of these quantities) of the rational tori at energy E. $\mu_1, \ldots, \mu_N$ need not be relatively prime, in order to allow for multiple repetitions of the POs. Also, at a given energy E, there might exist several POs with the same value of μ but different values of the amplitude A_μ. A completely worked-out, straightforward application of the trace formula in Eq. (5) to a 2D model of CS_2 can be found in [17]. A closer relation of Eq. (5) with rational tori is achieved by recalling, that for a PO:

$$\left(\frac{\partial S}{\partial E}\right)_{\text{PO}} = T_{\text{PO}} , \qquad S = \oint_{\text{PO}} \sum_{k=1}^{N} p_k \mathrm{d}q_k . \tag{6}$$

Moreover, for a rational torus μ, the action function S is just:

$$S = 2\pi\mu\mathfrak{I}_\mu . \tag{7}$$

So that, to first order in the energy E, Eq. (5) can be rewritten in the form:

$$n(E) \approx \sum_{\substack{\text{rational} \\ \text{tori}(\mu)\text{at}E}} A_\mu \cos(T_\mu E - \frac{\pi}{2}\mu\alpha + \frac{\pi}{4}\beta_\mu) \,. \tag{8}$$

It is important to emphasise again, that Eqs (5) and (8) involve only rational tori, that is ND POs, and completely neglect POs with lower dimension. An alternative approximation of the semiclassical density of states, which is more accurate than Eq. (5), is given in Eq. (24) of [3] for systems with $N = 2$ degrees of freedom. This uniform trace formula is written in the form:

$$n(E) \approx \sum_{\substack{\text{rational} \\ \text{tori}(\mu)\text{at}E}} (a_\mu \cos(2\pi\mu\,\mathfrak{I}_\mu - \frac{\pi}{2}\mu\alpha + \Delta_\mu) +$$

$$+ b_\mu \sin(2\pi\mu\,\mathfrak{I}_{\substack{\text{border} \\ \text{left}}} - \frac{\pi}{2}\mu\alpha) + c_\mu \sin(2\pi\mu\,\mathfrak{I}_{\substack{\text{border} \\ \text{right}}} - \frac{\pi}{2}\mu\alpha)) \,. \tag{9}$$

In Eq. (9), the subscripts "border left" and "border right" refer to the limits of the classically accessible phase space, which are usually 1D POs. The amplitudes a_μ, b_μ and c_μ and the additional phase $\Delta\mu$ now depend on the classical properties not only of the rational tori, but also of these 1D POs. More important for the purpose of this article, however, is the fact that Eq. (9) explicitly contains circular functions of the action integrals of the 1D POs. In the case, where these 1D POs correspond to a vanishing amplitude along the frequency W_2 and where the action integral $\mathfrak{I}_2$ always assumes the same value at the limits of the phase space, regardless of the value of the energy E, as is the case for the Hamiltonian in Eq. (16) [18, 19], one has:

$$S = 2\pi\,\mathfrak{I}_1 \qquad \left(\frac{\partial \mathfrak{I}_2}{\partial E}\right)_{\text{border}} = 0 \,. \tag{10}$$

Using Eqs (6) and (10), the uniform trace formula in Eq. (9) can then be rewritten to first order in energy in the most useful form:

$$n(E) \approx \sum_{\substack{\text{rational} \\ \text{tori}(\mu)\text{at}E}} (a_\mu \cos(T_\mu E - \frac{\pi}{2}\mu\alpha + \Delta_\mu) +$$

$$+ b_\mu \sin(\mu_1 T_{\substack{\text{border} \\ \text{left}}} E - \frac{\pi}{2}\mu\alpha) + c_\mu \sin(\mu_1 T_{\substack{\text{border} \\ \text{right}}} E - \frac{\pi}{2}\mu\alpha)) \,. \tag{11}$$

FT of the quantum and semiclassical density of states

The Fourier transform (FT) of a spectrum extending from $E_W-\Delta E/2$ to $E_W+\Delta E/2$ is taken in the form:

$$F(x,E_W) = \frac{1}{\sqrt{2\pi}} \int_{E_W-\Delta E/2}^{E_W+\Delta E/2} \mathrm{e}^{-j2\pi xE}\, g(E,E_W)\, n(E)\, \mathrm{d}E$$

$$g(E,E_W) = 1 - 4\left(\frac{E-E_W}{\Delta E}\right)^2 , \tag{12}$$

where $g(E,E_W)$ is the Welch windowing function, which is used to reduce the leakage at large time offsets. Other windowing functions, like Hanning, Parzen or Gaussian windows, could have been used as well. When dealing with the quantum spectrum, $n(E)$ in Eq. (12) is replaced by $\sum_k \delta(E-E_k)$, where $(E_1, E_2,\ldots)$ is the set of quantum eigenvalues. One simply gets:

$$F(x,E_W) = \frac{1}{\sqrt{2\pi}} \sum_k g(E_k,E_W)\, \mathrm{e}^{-j2\pi xE_k} . \tag{13}$$

E being expressed in reciprocal centimetres (cm^{-1}) and x being proportional to $1/E$, x is in centimetre units, and the abscissa is actually slightly modified, according to:

$$t[\mathrm{fs}] = \frac{x[\mathrm{cm}]}{c[\mathrm{cm\ fs}^{-1}]} \approx \frac{10^5 x}{3} , \tag{14}$$

in order to return to more usual femtosecond units for the abscissa.

Alternately, $n(E)$ in Eq. (12) can be replaced by one of the expressions in Eqs (8) or (11). Assuming that A_μ and T_μ remain mostly constant within each energy window $E_W-\Delta E/2 \le E \le E_W+\Delta E/2$, Fourier transformation of Eq. (8) leads to the conclusion that the squared modulus of the FT of the spectrum mainly displays peaks centred around values of x, such that:

$$x[\mathrm{cm}] = \frac{T_\mu[\mathrm{cm}]}{2\pi} = \frac{\mu_1}{W_1[\mathrm{cm}^{-1}]} = \ldots = \frac{\mu_N}{W_N[\mathrm{cm}^{-1}]} . \tag{15}$$

When using the modified abscissa scale in Eq. (14), peaks more simply appear around the periods T_μ (in femtoseconds) of the rational tori. Moreover, a single rational torus contributes to each peak, and the maximum intensity is just $(A_\mu \Delta E)^2/(18\pi)$. An exception occurs whenever the periods of two rational tori are too close together: in that case, some deviations might arise in the position and in the intensity of the peaks.

For a system with two degrees of freedom ($N=2$), Fourier transformation of the more accurate expression in Eq. (11) leads to a somewhat more complex picture: indeed, in addition to the peaks centred around the periods T_μ of rational tori, the squared modulus of the FT of the spectrum is seen to display other peaks centred around the periods $T_{\text{border left}}$ and $T_{\text{border right}}$ of the 1D POs at the limits of the classically accessible phase space and around the multiples of these periods. Again, a single trajectory contributes to each peak for rational tori, with a maximum intensity being just $(a_\mu \Delta E)^2/(18\pi)$. In contrast, all the rational tori with the same value of μ_1 contribute to the μ_1th repetition of the 1D POs, leading to a more complex intensity behaviour of these peaks. Also, deviations might arise in the expected position and intensity of the peaks whenever the periods of two POs, either 1D or 2D, are too close together (in the figures plotted in this article, the width of the peaks is about 4 fs).

The model Hamiltonian for CO_2

Suzuki [28] has shown that the vibrational levels of CO_2 can be correctly fitted up to about 10000 cm^{-1} above the ground level (about 13000 cm^{-1} above the bottom of the well) by diagonalising an effective Hamiltonian built according to:

$$\left\langle v_1, v_2^\ell, v_3 \middle| H \middle| v_1, v_2^\ell, v_3 \right\rangle = \sum_{i=1}^{3} \omega_i \left(v_i + \frac{d_i}{2} \right) + \sum_{i=1}^{3} \sum_{j=i}^{3} x_{ij} \left(v_i + \frac{d_i}{2} \right) \left(v_j + \frac{d_j}{2} \right) + x_{\ell\ell} \ell^2$$

$$\left\langle v_1, v_2^\ell, v_3 \middle| H \middle| v_1 - 1, v_2^\ell + 2, v_3 \right\rangle = -k_{12} \sqrt{v_1((v_2+2)^2 - \ell^2)} \,, \tag{16}$$

where $d_1 = d_3 = 1$ and $d_2 = 2$. ℓ is the vibrational angular momentum resulting from the twofold degeneracy of the bending mode 2, and 1 and 3 label respectively the symmetric and antisymmetric stretching motions. If v_2 is odd (respectively, even) then ℓ is odd (respectively, even). For the purpose of not complicating the discussion with arguments outside the scope of this paper (like the non-integrability of the exact Hamiltonian, or the influence of missing levels) and also of enabling the use of previous calculations, the quantum spectra, which will be considered in the next two sections, are obtained from the diagonalisation of the matrix in Eq. (16). In addition, the off-diagonal spectroscopic constants λ_1, λ_2 and λ_3, which were fitted by Suzuki [28], are discarded here for the sake of simplicity, whereas they could just be handled perturbatively along the same lines as y_{222} in [27]. The study of the complications arising from the study of a real experimental spectrum will be the aim of a

forthcoming paper [29]. Numerical values of the spectroscopic parameters given by Suzuki are the following (in cm^{-1}):

$$\begin{array}{lll} \omega_1 = 1349.97 & \omega_2 = 674.85 & \omega_3 = 2395.89 \\ x_{11} = -2.38 & x_{22} = -0.23 & x_{33} = -12.40 \\ x_{23} = -12.61 & x_{13} = -18.50 & x_{12} = 1.01 \\ k_{12} = 24.70 & x_{\ell\ell} = -0.38\ . & \end{array} \tag{17}$$

Using the correspondence relation between quantum and classical mechanics, the classical analogue of the quantum Hamiltonian in Eq. (16) is, for $\ell = 0$ [27]:

$$E \equiv H(I_1, I_2, I_3, \varphi_1, \varphi_2, \varphi_3) = \sum_{i=1}^{3} \omega_i I_i + \sum_{i=1}^{3} \sum_{j=i}^{3} x_{ij} I_i I_j + 2k_{12} I_1^{1/2} I_2 \cos(\varphi_1 - 2\varphi_2)\ ,$$

$$q_i = \sqrt{2I_i}\cos\varphi_i\ , \qquad p_i = -\sqrt{2I_i}\sin\varphi_i\ , \tag{18}$$

where the (I_i, φ_i) are conjugate, action-angle like coordinates. As in [27], all the classical calculations are done for a semiclassical quantum number associated with the vibrational angular momentum equal to $L = \ell = 0$, thus neglecting the quantum selection rule dealing with the parity of v_2 and ℓ. Since the expression of the energy in Eq. (18) does not depend on φ_3, $\mathcal{I}_3 = I_3$ is an action integral of the system, which is associated with a Maslov index $\alpha_3 = 2$:

$$\mathcal{I}_3 = I_3 = v_3 + \frac{1}{2}\ . \tag{19}$$

The Hamiltonian is next rewritten in the form:

$$E' = \sum_{i=1}^{2} \omega_i' I_i + \sum_{i=1}^{2} \sum_{j=i}^{2} x_{ij} I_i I_j + 2k_{12} I_1^{1/2} I_2 \cos(\varphi_1 - 2\varphi_2)\ ,$$

$$E' = E - \omega_3 I_3 - x_{33} I_3^2\ , \qquad \omega_i' = \omega_i + x_{i3} I_3\ . \tag{20}$$

One is thus led to the expression of a 2D resonance Hamiltonian, the classical mechanics of which has been studied recently in some details [18, 19]. The calculations will not be reproduced here. Let us just mention some key results: the first action integral of the Hamiltonians in Eqs (18) and (20) is $\mathcal{I}_1 = I = 2I_1 + I_2$, which is associated with a Maslov index $\alpha_1 = 8$ [27]:

$$\mathcal{I}_1 = I = 2I_1 + I_2 = 2v_1 + v_2 + 2\ . \tag{21}$$

The last action integral $\mathcal{I}_2$ can be expressed as a function of E' and I, that is of E, $\mathcal{I}_1$ and $\mathcal{I}_3$ [18, 19]. It is associated with a Maslov index $\alpha_2 = 2$, but has no quantum

counterpart like Eqs (19) or (21). The classical frequencies associated with $\mathcal{I}_1 = I$ and $\mathcal{I}_2$ are $W_1 = \nu^*$ and $W_2 = \omega^*$, whose expressions are given in [18, 19]. The expression of the third classical frequency is obtained along the same lines as ν^*, leading to:

$$W_3 = \nu_3^* = \omega_3 + 2x_{33}I_3 + x_{23}I + \frac{1}{T}\left(\frac{x_{13}}{2} - x_{23}\right)\int_0^T J(t)\mathrm{d}t$$

$$= \omega_3 + 2x_{33}I_3 + x_{23}I + \left(\frac{x_{13}}{2} - x_{23}\right)\left(\beta + (\alpha - \beta)\frac{\Pi(\eta|\mu)}{K(\mu)}\right). \qquad (22)$$

Symbols have the same meaning as in [18, 19].

Assignment of the FT of the 2D spectrum of CO_2

All the tools, which are needed to connect the classical POs of CO_2 to the FT of its spectrum, are now at one's disposal. In this section, the FT of the 2D spectrum will be investigated, whereas the FT of the 3D spectrum will be handled in the following section. By "2D spectrum", we mean the spectrum obtained by freezing two quantum numbers in Eq. (16). More precisely, in the following of this article the 2D spectrum will consist of those levels with $v_3 = 0$ and $\ell = 0$ or $\ell = 1$, according to the parity of v_2. Eq. (19) shows that the classical Hamiltonian corresponding to the 2D spectrum is obtained by replacing I_3 by 1/2 in Eq. (20). In the "3D spectrum", v_3 is left free to vary, whereas the condition $\ell = 0$ or $\ell = 1$ is maintained.

The squared modulus of ten FTs of the 2D quantum spectrum of CO_2 is drawn in Fig. 1 for times lower than 300 fs. In this figure, the centre E_W of the energy window increases from 4000 cm^{-1} to 8500 cm^{-1} with increments of 500 cm^{-1}, the width of each window being $\Delta E = 8000$ cm^{-1}. Each peak appearing in this figure will be associated with a classical PO. The discussion will essentially deal with the abscissa of the peaks (that is, the period of the PO), whereas their intensity will only be discussed qualitatively.

The typical behaviour of the classical frequencies $W_1 = \nu^*$ and $W_2 = \omega^*$ at a given energy E is illustrated in Fig. 2 (top). The classical frequencies are drawn as a function of the first action integral $\mathcal{I}_1 = I$. For 2D CO_2, each set (E, I) defines a single torus. Without entering into details, it is to be noted that this point was not obvious *a priori* and results from the fact that CO_2 can assume the phase space structures labelled II/III and II/*h* in [19], but not the II/III/*h* phase space structure.

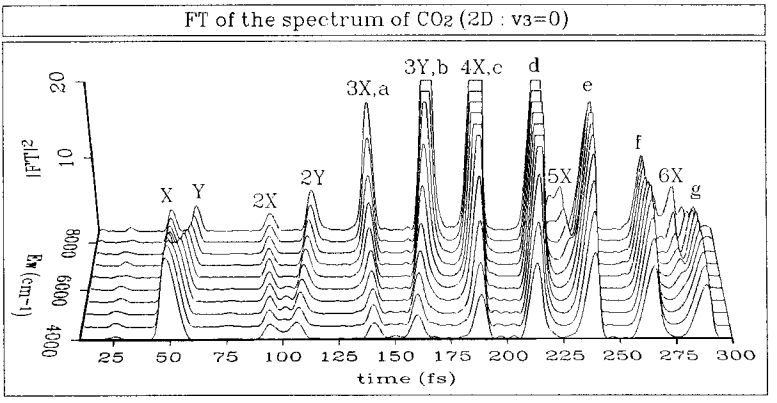

Fig. 1. Squared modulus of 10 Fourier transforms of the 2D quantum spectrum of CO_2 for times up to 300 fs. The quantum spectrum is obtained by diagonalisation of the Hamiltonian matrix in Eq. (16). Each Fourier transform is calculated according to Eq. (13), with an energy E_W at the center of the window increasing from 4000 cm^{-1} to 8500 cm^{-1} (increments of 500 cm^{-1}) and a window width $\Delta E = 8000$ cm^{-1}. Abscissas are rescaled according to Eq. (14). Each peak in the FT is associated with a PO, either the repetition of a 1D PO ($X = 1D(I_{min})$, $Y = 1D(I_{max})$) or a rational torus ($a = 1:3^L$, ..., $g = 1:6^L$)

In addition, the phase space structure II/III appears only marginally (for low values of I), so that the vast majority of the plots of the classical frequencies versus I look like that one at $E = 8000$ cm^{-1}, which is given in Fig. 2. These plots are characterised by:
(i) a finite range of permitted values of I. The minimum and maximum values I can reach, $I_{min}(E, I_3)$ and $I_{max}(E, I_3)$, can be calculated by finding the roots of a polynome and are known to be associated with elliptic fixed points [19] both in the (p_1, q_1) and (p_2, q_2) Poincaré surfaces of section. These elliptic fixed points correspond to a vanishing amplitude of motion along the frequency ω^* and, since $N = 2$, are 1D POs, which we label $1D(I_{min})$ and $1D(I_{max})$.
(ii) a cusp-like decrease to zero of ω^* and a vertical tangent in the plot of ν^* on both sides of a value $I^+(E, I_3)$ of I, which can be determined according to:

$$E - \omega_3 I_3 - x_{33} I_3^2 = \frac{\omega_1 + x_{13} I_3}{2} I^+ + \frac{x_{11}}{4} I^{+2} . \tag{23}$$

I^+ appears as an hyperbolic fixed point separatrix in the (p_i, q_i) surfaces of section and is a 1D PO. Unless using another uniform trace formula, which would properly take into account the coalescence of rational tori at the separatrix and would therefore be still more accurate and complex than the trace formula in Eq. (9), this kind of PO, however, plays no role in Berry and Tabor's trace formula for integrable systems.

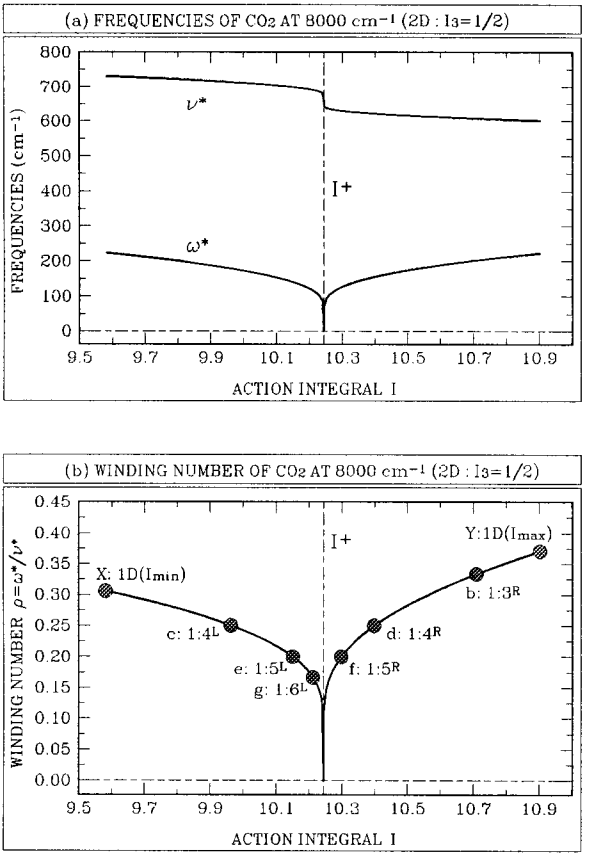

Fig. 2. Plot, as a function of the first action integral $\mathcal{I}_1 = I$, of the classical frequencies $W_1 = \nu^*$ and $W_2 = \omega^*$ (top) and of the winding number $\rho = \omega^*/\nu^*$ (bottom) of CO_2 at energy $E = 8000$ cm^{-1}. I_3 is equal to 1/2, because these plots are used to find the POs which appear in the FT of the 2D spectrum of CO_2. The 1D POs and the rational tori with period shorter than 300 fs are indicated in the bottom plot

Rational tori are then easily found by seeking for the rational values μ_2/μ_1 of the winding number $\rho = \omega^*/\nu^*$, which is plotted in Fig. 2 (bottom) at energy $E = 8000$ cm^{-1}. Due to the cusp at the I^+ separatrix, there often exist two rational tori with the same value of $\rho = \mu_2/\mu_1$, one for values of I smaller than I^+ and one for values of I larger than I^+. These rational tori are labelled respectively $\mu_2 : \mu_1{}^{\mathrm{L}}$ and $\mu_2 : \mu_1{}^{\mathrm{R}}$. The six rational tori having a period T_μ shorter than 300 fs at $E = 8000$ cm^{-1} are indicated in Fig. 2 (bottom).

In Fig. 3 are drawn, on the same diagram, the time values corresponding to the maxima of the peaks in the FT of the quantum spectrum (open circles), the repetitions of the periods of the 1D POs (dashed lines) and the periods of the rational tori (solid lines) up to 300 fs. It is seen that all the quantum open circles fall on one of the classical lines, so that the period of a PO can be assigned to each peak in the FT of the spectrum. A small deviation occurs for the peaks around 275 fs, which is due to the crossing (as a function of energy) of the periods of two 1D POs. The upper time limit of 300 fs was precisely chosen, in order not to have to deal with too many crossing periods, which complicate the interpretation of the FT of the semiclassical density of states. As energy increases, the limiting values of ρ at $I_{\min}$ and $I_{\max}$ also increase, and rational tori successively enter the classically accessible region $I_{\min} \leq I \leq I_{\max}$. Of course, the higher the value of μ_2/μ_1, the higher the value of the energy where the rational torus becomes real. Anyway, a rational torus always enters the classically accessible region as the corresponding value of ρ crosses $I_{\min}$ or $I_{\max}$.

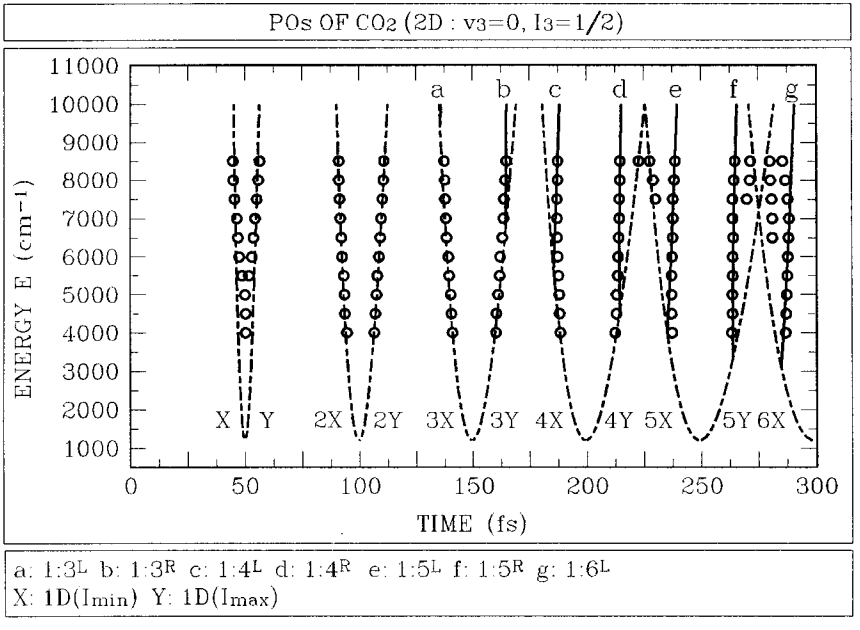

Fig. 3. Plot, for increasing values of the energy E, of the time values shorter than 300 fs corresponding to (i) the maxima of the peaks in the FTs of the 2D quantum spectrum of CO_2 (energy window centred at $E_W=E$) (open circles), (ii) the repetitions of the periods of the 1D POs (dashed lines), (iii) the periods of the rational tori (solid lines). This figure shows that each peak in the FT of the quantum spectrum corresponds to the period of a classical PO

This is the reason, why the solid lines associated with rational tori in Fig. 3 always start on the dashed lines associated with the repetitions of the 1D POs. Also, one can observe in Fig. 3, that the periods of 2D POs (rational tori) vary much more slowly with energy than the periods of 1D POs. Further studies are needed to better understand this point.

Actually, complex rational tori can be included in the uniform trace formula in Eqs (9) and (11) [3]. Complex rational tori are complex solutions of Hamilton's equations with real values of the action integrals and of the classical frequencies. Their expressions are given in [17] for the 1 : 2 resonance Hamiltonian. Accordingly, a rational torus does contribute to the FT of the spectrum even before entering the classically allowed region. However, due to the exponential decrease of a_μ when going from the classically authorised to the classically forbidden region [3], the contribution of a complex rational torus to the FT of the spectrum is negligible far from the energy where the rational torus becomes real. Near to the value of E where the complex rational torus becomes real, the contribution of the complex rational torus might in turn wipe out that of the repetition of the 1D PO, but one is then no longer able to distinguish between the two periods, which are very close together. The exponential growth of a_μ is clearly seen in Fig. 1, for instance for the peaks labelled a, b, c and d, which are associated with the $1:3^{\mathrm{L}}$, $1:3^{\mathrm{R}}$, $1:4^{\mathrm{L}}$ and $1:4^{\mathrm{R}}$ rational tori. After this exponential growth, the intensity of each peak remains almost constant, as long as the rational torus remains sufficiently far both from the limits $I_{\min}$ and $I_{\max}$ and from the separatrix I^+. This can be checked in Fig. 1 for the peaks labelled e and f, which are associated respectively with the rational tori $1:5^{\mathrm{L}}$ and $1:5^{\mathrm{R}}$. In contrast, the expression of a_μ in [3] shows that a_μ again diminishes as the rational torus approaches too closely the separatrix, because of the curvature of the second action integral $\Im_2$ as a function of I. This is what happens to the $1:6^{\mathrm{L}}$ rational torus, which is labelled g in Fig. 1. As already stated above, the intensity of peaks associated with 1D POs is much more complex to analyse, since all the rational tori with the same value of μ_1 contribute to the μ_1th repetition of the 1D PO. One however observes in Fig. 1, that the intensity of 1D POs varies slowly and is not at all negligible compared to the intensity of 2D POs, except for the rational tori with the lowest values of μ, like 1 : 3 and 1 : 4.

For the sake of being complete, the (p_1,q_1) and (p_2,q_2) Poincaré surfaces of section of all the POs which have been discussed in this section are represented in Fig. 4 at energy $E = 8000$ cm^{-1}. In contrast with the trajectories with irrational values of the winding number ρ, which appear as continuous, non intersecting lines in the

surfaces of section, rational tori appear as a finite number of points in each section. Typically, a $1:\mu_1$ rational torus consists of μ_1 points in the (p_1, q_1) surface of section and $2\mu_1$ points in the (p_2, q_2) surface of section. In addition, as already stated above, the 1D POs are the elliptic points at the centre of each island. The peaks in the FT of the 2D spectrum centred at 8000 cm^{-1} in Fig 1 are the periods of the trajectories plotted in this figure.

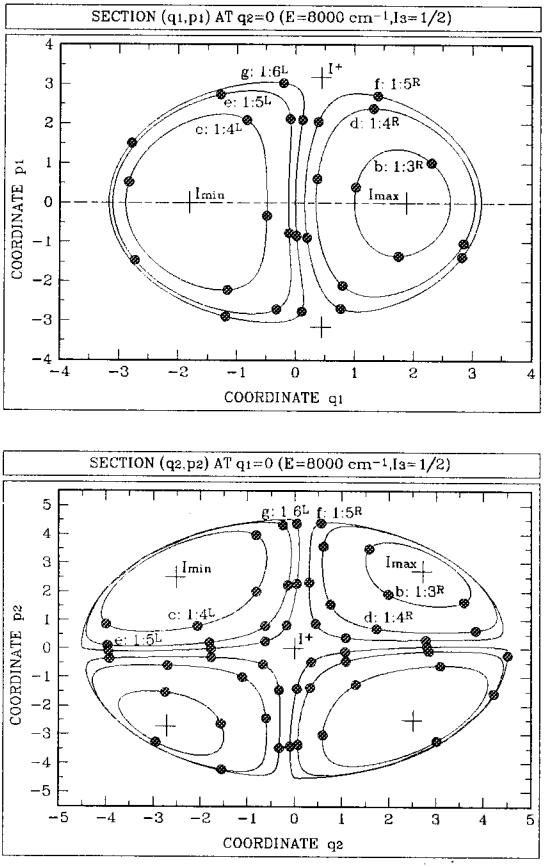

Fig. 4. Poincaré surfaces of section at energy E=8000 cm^{-1} and for I_3=1/2 of the 1D and 2D POs of CO_2 with period shorter than 300 fs. The elliptic fixed points I_{min} and I_{max} are the 1D POs discussed in the text. In contrast, the hyperbolic fixed point I^+ plays no role in the uniform trace formula used in this article. The rational tori appear as a finite number of points in each section. For the sake of eye guidance, a trajectory very close to the PO but with an irrational value of ρ is drawn for each rational torus. The peaks, which appear in the FT of the 2D spectrum in Fig. 1 (energy window centred centred at 8000 cm^{-1}), correspond to the periods of the trajectories drawn in this figure

Assignment of the FT of the 3D spectrum of CO_2

The squared modulus of eleven FTs of the 3D quantum spectrum of CO_2 is drawn in Fig. 5 for times lower than 300 fs. In this figure, the centre E_W of the energy window increases from 4000 cm^{-1} to 9000 cm^{-1} with increments of 500 cm^{-1}, the width of each window being $\Delta E = 8000$ cm^{-1}. This figure is quite similar to the same drawing for the 2D quantum spectrum in Fig. 1, but with some additional peaks. The aim of this section is to discuss the reasons for the similarities and differences between the FTs of the 2D and 3D spectra.

The most obvious difference arises from the fact, that in the three dimensional case there exist three classical frequencies, each one depending on three action integrals, instead of only two frequencies depending on two action integrals. At a given energy E, each frequency still depends on two action integrals, for instance $\mathfrak{I}_1 = I$ and $\mathfrak{I}_3 = I_3$. However, for given values of E and I_3, the classically accessible phase space just consists of a quite narrow band around $I = I^+(E, I_3)$, so that the three frequencies are more conveniently plotted as a function of $I - I^+(E, I_3)$ and I_3, rather than simply of I and I_3. Such a plot of the three classical frequencies of CO_2 is shown in Fig. 6 at $E = 9000$ cm^{-1}. As a consequence of its expression in Eq. (22), it is

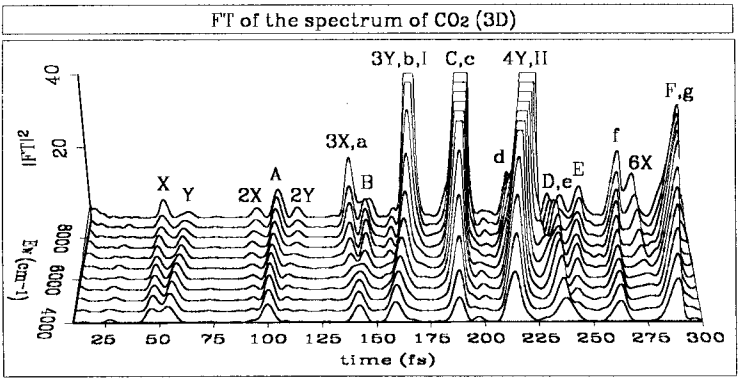

Fig. 5. Squared modulus of 11 Fourier transforms of the 3D quantum spectrum of CO_2 for times up to 300 fs. The quantum spectrum is obtained by diagonalisation of the Hamiltonian matrix in Eq. (16). Each Fourier transform is calculated according to Eq. (13), with an energy E_W at the center of the window increasing from 4000 cm^{-1} to 9000 cm^{-1} (increments of 500 cm^{-1}) and a window width $\Delta E = 8000$ cm^{-1}. Abscissas are rescaled according to Eq. (14). Each peak in the FT is associated with a PO, which is one of: (i) the repetition of a 1D PO (X=1D(I_{min}, I_3=0), Y=1D(I_{max}, I_3=0)), (ii) a 2D PO along the I_3=0 edge (a=2D(I_3=0,1:3^L),..., g=2D(I_3=0,1:6^L)), (iii) a 2D PO along the two other edges of the classically accessible phase space (A=2D(I_{min},7:2),..., F=2D(I_{min},20:6)) or (iv) a rational torus (I=3D(1:3:11^R) and II=3D(1:4:15^R))

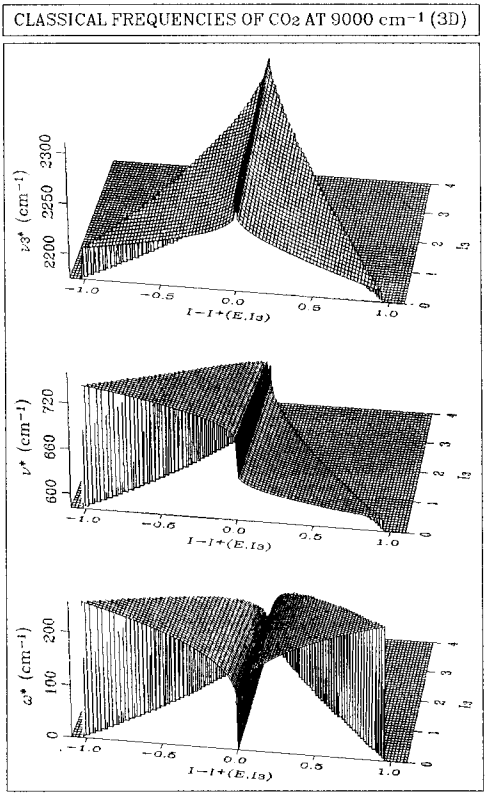

Fig. 6. Plot, as a function of I–$I^+(E,I_3)$ and I_3, of the classical frequencies $W_1=\nu^*$, $W_2=\omega^*$ and $W_3=\nu_3{}^*$ of CO_2 at energy E=9000 cm^{-1}

clearly seen in this figure that the plot of the additional frequency $\nu_3{}^*$, like those of ω^* and ν^*, displays a vertical tangent at $I=I^+(E,I_3)$. Moreover, the width of the classically accessible phase space in the I direction diminishes as the value of I_3 increases, leading to an almost triangular shape of the accessible phase space.

3D rational tori are then characterised not only by a rational value of the winding number $\rho=\omega^*/\nu^*$, but also by a rational value of the additional winding number $\rho'=\nu_3{}^*/\nu^*$. These two winding numbers are plotted in Fig. 7 at $E=9000\,\text{cm}^{-1}$. Looking for 3D rational tori amounts to finding the points where both surfaces are rational. The key point, however, consists in noticing that a 3D rational torus defined by two winding numbers $\rho=\mu_2/\mu_1$ and $\rho'=r/s$ is associated with the vector $\mu=(s\mu_1, s\mu_2, r\mu_2)$ whenever s and μ_2 are prime together, and therefore has a period T_μ which is equal to s times the period of the 2D torus with the same value of ρ.

Since the rational value with the lowest value of s, which is observed for ρ', is $\rho'=7/2$ close to the separatrix and $\rho'=10/3$ somewhat further from the separatrix, it follows from the observation above and from the study of the 2D spectrum in the previous section, that almost no 3D rational tori have a period shorter than 300 fs for CO_2. In contrast with the 2D case, almost none of the peaks observed below 300 fs in the FTs of the 3D spectrum of CO_2 is associated with a rational torus. Only two rational tori are actually computed, with classical frequencies $\omega: \nu^*: \nu_3^*$ in the respective ratios 1 : 3 : 11 and 1 : 4 : 15 and periods around 164 fs and 220 fs.

The trace formula in Eqs (5) and (8) is therefore of little help, and drawing a parallel between the FT of the 3D quantum spectrum and the periods of the classical

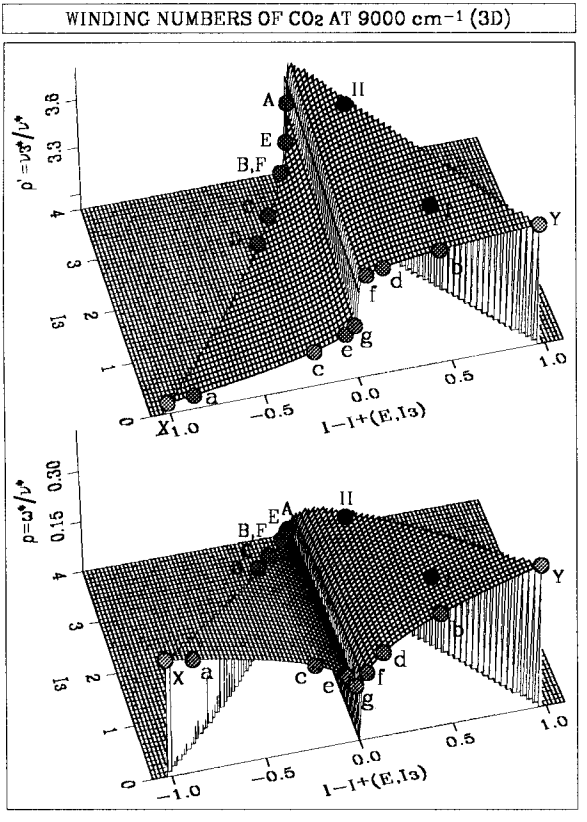

Fig. 7. Plot, as a function of I–$I^+(E,I_3)$ and I_3, of the two winding numbers $\rho=\omega^*/\nu^*$ and $\rho'=\nu_3^*/\nu^*$ of CO_2 at energy $E=9000$ cm^{-1}. The POs with period shorter than 300 fs are indicated. The fact that there exist only two 3D rational tori having a period shorter than 300 fs results in almost all the dots, which symbolise the POs, lying along the borders of the classically accessible phase space

POs with lower dimension (2D and 1D POs) requires the extension of the uniform trace formula in Eqs (9) and (11) to the 3D case. This will not be done here. However, it will be shown in the remaining of this section, that almost all the peaks in the FT can indeed be associated with the periods of 2D and 1D POs. 2D POs are those trajectories located on the edges of the almost triangular accessible phase space, that is those trajectories, which satisfy either $I_3 = 0$, or $I = I_{\min}(E, I_3)$, or $I = I_{\max}(E, I_3)$. If $I_3 = 0$, then the motion along the frequency ν_3^* vanishes and there only remains to seek for a rational value of ρ. Similarly, if $I = I_{\min}(E, I_3)$ or $I = I_{\max}(E, I_3)$, the motion along the frequency ω^* vanishes and there only remains to seek for a rational value of ρ'. These 2D POs are labelled respectively $2D(I_3 = 0, \mu_2 : \mu_1^{L \text{ or } R})$ and $2D(I_{\min} \text{ or } I_{\max}, \mu_3 : \mu_1)$. Two of the corners of the triangular shape, that is the trajectories with $I_3 = 0$ and $I = I_{\min}$ or $I_{\max}(E, I_3 = 0)$, are 1D POs, since the

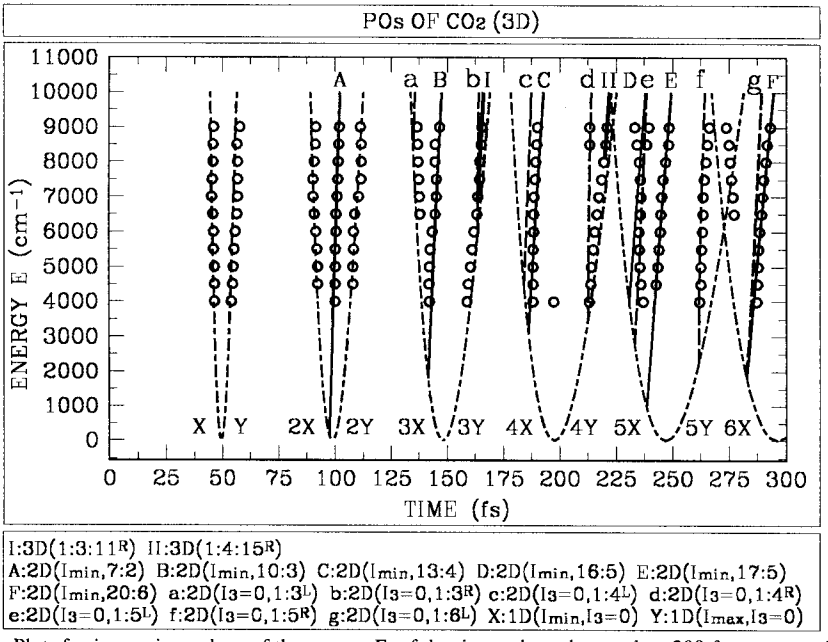

Fig. 8. Plot, for increasing values of the energy E, of the time values shorter than 300 fs corresponding to (i) the maxima of the peaks in the FTs of the 3D quantum spectrum of CO_2 (energy window centred at $E_W = E$) (open circles), (ii) the repetitions of the periods of the 1D POs (alternate dashed lines), (iii) the periods of the 2D POs lying on the $I_3 = 0$ edge (solid lines), (iv) the periods of the 2D POs lying on the $I = I_{\min}(E, I_3)$ and $I = I_{\max}(E, I_3)$ edges (long dashed lines), (v) the periods of the rational tori (broad solid lines). This figure shows that each peak in the FT of the quantum spectrum corresponds to the period of a classical PO.

motion vanishes both along the ω^* and the ν_3^* frequencies. These 1D POs are labelled 1D(I_{min} or I_{max}, $I_3=0$). It is to be noted, that the 2D POs along the $I_3=0$ border have periods close to the periods of the rational tori in the 2D case, since there only exists a small difference in the value of I_3 (0 against 1/2). For the same reason, the 1D POs have very similar periods for both the 2D and 3D spectra. Therefore, it is concluded that the additional peaks, which are observed in Fig. 5 compared to Fig. 1 and were not assigned to rational tori, are most likely due to the 2D POs lying along the two other edges of the triangle, that is those labelled 2D(I_{min} or I_{max}, $\mu_3:\mu_1$). This is actually what is observed in Fig. 8, where the periods of the classical 2D and 1D POs are drawn on the same diagram as the time values associated with the maxima of the peaks in the FTs of the 3D spectrum of CO_2. In particular, the very clear additional peaks that appear around 100, 145 and 245 fs in Fig. 5 are seen to be due to the 2D(I_{min},7:2), 2D(I_{min},10:3) and 2D(I_{min},17:5) POs.

References

[1] DELORY, J. M., TRIC, C.: *Chem. Phys.*, **3**, 54 (1974)
[2] LEVIANDIER, L., LOMBARDI, M., JOST, R., PIQUE, J. P.: *Phys. Rev. Letters*, **56**, 2449 (1986)
[3] BERRY, M. V., TABOR, M.: *Proc. Roy. Soc.*, **A349**, 101 (1976)
[4] GAO, J., DELOS, J. B.: *Phys. Rev.*, **A49**, 869 (1994)
[5] GUTZWILLER, M. C.: *J. Math. Phys.*, **12**, 343 (1971)
[6] GUTZWILLER, M. C.: *Phys. Rev. Letters*, **45**, 150 (1980)
[7] GUTZWILLER, M. C.: *J. Phys. Chem.*, **92**, 3154 (1988)
[8] BALAZS, N. L., VOROS, A.: *Phys. Rep.*, **143**, 109 (1986)
[9] GUTZWILLER, M. C.: *Physica D*, **5**, 183 (1982)
[10] TABOR, M.: *Physica D*, **6**, 195 (1983)
[11] WINTGEN, D.: *Phys. Rev. Letters*, **58**, 1589 (1987)
[12] DU, M. L., DELOS, J. B.: *Phys. Rev. Letters*, **58**, 1731 (1987)
[13] GASPARD, P., ALONSO, D.: *Phys. Rev.*, **A47**, 3468 (1993)
[14] BURGHARDT, I., GASPARD, P.: *J. Chem. Phys.*, **100**, 6395 (1994)
[15] OZORIO DE ALMEIDA, A. M.: *Lect. Notes Phys.*, **263**, 197 (1986)
[16] TOMSOVIC, S., GRINBERG, M., ULLMO, D.: *Phys. Rev. Letters*, **75**, 4346 (1995)
[17] JOYEUX, M.: *Chem. Phys. Letters*, **247**, 454 (1995)
[18] JOYEUX, M.: *Chem. Phys.*, **185**, 263 (1994)
[19] JOYEUX, M.: *Chem. Phys.*, **203**, 281 (1996)
[20] GASPARD, P., ALONSO, D., BURGHARDT, I., In *Advances in Chemical Physics*, Vol. XC, (Eds I. PRIGOGINE, S.A. RICE), Wiley, 1995, p. 105
[21] EZRA, G. S.: *J. Chem. Phys.*, **104**, 26 (1996)
[22] ROUBEN, D. C., EZRA, G. S.: *J. Chem. Phys.*, **103**, 1375 (1995)
[23] HIRAI, K., HELLER, E. J., GASPARD, P.: *J. Chem. Phys.*, **103**, 5970 (1995)
[24] BARANGER, M., HAGGERTY, M. R., LAURITZEN, B., MEREDITH, D. C., PROVOST, D.: *Chaos*, **5**, 261 (1995)

[25] EINSTEIN, A.: *Ver. Deutsch. Phys. Ges.*, **19**, 1982 (1917)
[26] JOYEUX, M.: *J. Chem. Phys.*, **102**, 2816 (1995)
[27] JOYEUX, M.: *J. Mol. Spectr.*, **175**, 262 (1996)
[28] SUZUKI, I.: *J. Mol. Spectr.*, **25**, 479 (1968)
[29] MICHAILLE, L., RING, H., SITJA, G., PIQUE, J. P.: *Phys. Rev. Letters*, **78**, 3848 (1997)

COMMENTS

MARTIN GRUEBELE:

It is very interesting to us that JM should concentrate explicitly on contributions of low-D vs. *N*-D periodic orbits. These appear to be the semiclassical analogs of edge and interior states defined in Bigwood and Gruebele ref. [23].

In particular, 1D POs are related to the pure overtone transitions often observed experimentally and commonly taken as the standard benchmark for IVR. 2D and 1D POs seem to enjoy enhanced stability even at higher energies in CO_2, given that they dominate the spectra in Fig. 7 of Joyeux and Michaille.

It would be very interesting to see an analysis of the motions that eventually cause low-D POs to be unstable, compared to the highly resonant overlaps that probably occur for high-D POs.

REPLY

Properly speaking, periodic orbits (POs), which appear in the Fourier transform of the spectra and are the principal objects in trace formulae theories, are not states. The semiclassical analogues of quantum states are the trajectories that obey the so-called Einstein–Brillouin–Keller (EBK) quantization rules, which put conditions on action integrals rather than classical frequencies. Nonetheless, there do exists a link between the 'edge' states of Bigwood and Gruebele and the periods of the low dimensional POs: intuitively, states located near the limits of the classically accessible phase space (that is at one side of the quantum polyad) are likely to be also 'edge' states in the sense of Bigwood and Gruebele, since they probably strongly couple to only half the number of levels to which a state at the center of the classical region (or the quantum polyad) effectively couples - simply because the levels on its other side do not exist. Now, energy can be expanded to first order in the form :

$$E \approx W_1 I_1 + W_2 I_2 + \ldots = \nu^* I + \omega^* \mathfrak{I}_2 + \ldots$$

and states located nearest to the limits of the classical region (that is to the 1D POs for the 2D system, or to the 2D POs for the 3D system) are defined by the same

values of $\mathfrak{I}_2$ (1/2 or -1/2, see Fig. C1) and integral values of I. Therefore, it follows that two such neighboring states are separated by a gap which is approximately equal to the frequency ν^* for each state, and also - because of the limited curvature away from the separatrix - to the frequency ν^* at the PO, that is precisely 2π divided by the period of the 1D or 2D PO.

A last point worth noting on this topic, is that each level is coupled to very few other ones at these relatively low energy values: polyad $i=7$ (centered at about 7200 cm^{-1}) contains only 4 levels and polyad $i=8$ (centered at about 7700 cm^{-1}) only 5 levels, so that the discrimination between edge and interior states is statistically rather meaningless. In Table I below are given for example the eigenvectors for each level of polyad $i=8$, $v_3=0$ and $\ell=0$ ($I=10$, $I_3=1/2$, $L=0$). At higher energies this discrimination however probably becomes more meaningfull.

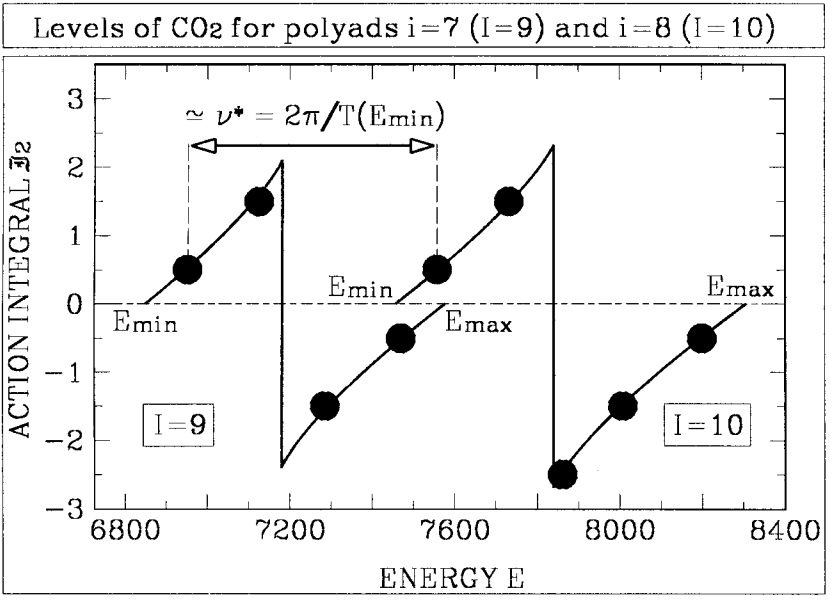

Fig. C1. Plot of the last action integral $\mathfrak{I}_2$ as a function of energy E for the trajectories with $(I, L, I_3)=(9,0,1/2)$ and $(10,0,1/2)$. The black dots represent the quantum levels of the corresponding polyads $(i, \ell, v_3)=(7,0,0)$ and $(8,0,0)$, located at the matching half-integral values of $\mathfrak{I}_2$. For each value of I, the minimum and maximum values of E are the elliptic fixed points 1D POs of the 2D problem. Notice that semiclassical levels close to the limits of the classical region (for a given value of I) and to the 1D POs have values of $\mathfrak{I}_2$ equal to 1/2 or -1/2. The gap between two such points is approximately the frequency ν^* at the 1D PO

Table I

Eigenvectors of polyad $(i, \ell, v_3) = (8,0,0)$. Corresponding classical action integrals are $(I, L, I_3) = (10,0,1/2)$. The last action integral $\mathcal{I}_2$ is indicated for each quantum level

Quantum level $\longrightarrow$	7556.20	7730.59	7861.61	8006.78	8198.46
$\mathcal{I}_2 \longrightarrow$	1/2	3/2	-5/2	-3/2	-1/2
$\downarrow \vert v_1, v_2\rangle$					
$\vert 0,8\rangle$	0.389	-0.485	0.471	-0.504	0.370
$\vert 1,6\rangle$	-0.613	0.336	-0.014	-0.355	0.620
$\vert 2,4\rangle$	0.580	0.218	-0.443	0.260	0.594
$\vert 3,2\rangle$	-0.350	-0.604	0.068	0.626	0.341
$\vert 4,0\rangle$	0.117	0.489	0.760	0.401	0.098

Let us now turn to the question of the stability of low dimensional periodic orbits. The Hamiltonian used in our contribution is an integrable one, which implies a very limited number of bifurcations and no chaos at all. The bifurcations actually occur for the triple roots of $(\mathrm{d}J/\mathrm{d}t)^2$ in Eqs (2.5) and (2.6) of [19]. Using the numerical values in Eq. (17) of our contribution, this means that, for $v_3 = 0$ ($I_3 = 1/2$), a first bifucation is observed at ($E = 1196.65$ cm^{-1}, $I = 0.0027$), that is well below the ground state at 2533.43 cm^{-1}. At this tangent bifurcation, the hyperbolic fixed point separatrix and one elliptic fixed point 1D PO are created, that one with highest value of E and lowest value of I. Using the terminology of [19], the phase space structure undergoes a transition from II/III to II/h. The next bifurcation is found at $E = 178926$ cm^{-1} and $I = 426.8$, which can be considered - with a not too bad uncertainty - to be meaningless!

Concerning chaos, the Kolmogorov-Arnold-Moser (KAM) theorem states that all rational tori are destroyed upon addition of the slightest non integrable perturbation, but that almost all the other tori are preserved. In particular, low dimensional POs are not automatically distroyed by the slightest perturbation, since they are not rational tori. Moreover, macroscopic chaos, which is associated with resonance islands overlaps, would primarily develop around the separatrix, because of the derivative of the winding number, which appears in the expression for resonance islands widths [1]. The regions around the elliptic fixed points POs appear to the most stable ones with that respect. A recent study on CO_2 using a non integrable Hamiltonian [2, 3] shows that for an energy close to 10000 cm^{-1} there only exists a very thin region of macroscopic chaos around the separatrix.

[1] JOYEUX, M.: *J. Phys. A., Math. Gen.*, **29**, 5963 (1996)
[2] JOYEUX, M.: *J. Chem. Phys.*, **221**, 269 (1997)
[3] JOYEUX, M.: *J. Chem. Phys.*, **221**, 287 (1997)